Available online at www.sciencedirect.com

SciVerse ScienceDirect

Journal of the European Ceramic Society 32 (2012) 2145–2151

www.elsevier.com/locate/jeurceramsoc

Ruby micro-piezospectroscopy in $GdAlO_3/Al_2O_3(/ZrO_2)$, $Er_3Al_5O_{12}/Al_2O_3(/ZrO_2)$ and $Y_3Al_5O_{12}/Al_2O_3(/ZrO_2)$ binary and ternary directionally solidified eutectics

Gwénaël Gouadec [a,*], Karim Makaoui [a], Loïc Perrière [b,c], Philippe Colomban [a], Léo Mazerolles [b]

[a] *LADIR (UMR 7075), CNRS, Univ. P. et M. Curie (UPMC – Paris 6), 4 Place Jussieu, 75252 Paris Cedex 05, France*
[b] *ICMPE (UMR 7182), CNRS, Univ. Paris Est Créteil (UPEC – Paris 12), 2 rue H. Dunant, 94320 Thiais, France*
[c] *ONERA, DMSC, 29 avenue de la Division Leclerc, BP72, FR-92322, Châtillon Cedex, France*

Received 12 July 2011; received in revised form 6 January 2012; accepted 18 January 2012
Available online 15 March 2012

Abstract

The fluorescence from (naturally present) Cr^{3+} impurities was used to measure the residual stress in the alumina phase of six melt-grown ceramic eutectic composites associating gadolinum aluminum perovskite (GAP), erbium aluminum garnet (EAG) or yttrium aluminum garnet (YAG) with α-alumina and cubic zirconia. Such measurements are reported for the first time in the GAP containing eutectics.

In the usual hydrostatic assumption, we conclude to a residual compression in the range of ∼70–400 MPa depending on the sample composition. The validity of the hydrostatic assumption is questioned when a microscope is used for the measurements.

Keywords: Al_2O_3; Non-destructive evaluation; Residual stress; Piezospectroscopy; Directionally solidified eutectics

1. Introduction

Directionally solidified eutectic (DSE) ceramic oxides are high melting point interlocking distributions of oxidation resistant single crystals, exhibiting remarkable strength and creep resistance.[1–3] They are developed in view of high-temperature structural applications such as turbine blades and reliability will strongly depend on the initial level of residual stress. In DSEs incorporating a ruby phase (*i.e.* a chromium-doped α-alumina single crystal), R_1 and R_2 fluorescence bands can be used to monitor this stress, with the advantage of precise and easy impact point selection.[2] These bands shift under stress as a result of Cr^{3+} ligand field modification and have been used since 1986 for pressure calibration in diamond anvil cells.[4] If the stress is expressed in an arbitrary orthogonal frame and does not exceed 20 GPa, then the wavenumber shifts can be approximated with the following relation[5,6]:

$$\Delta\bar{\nu}_{R_n} = \sum_{i,j=1}^{3} (\Pi_{ij}^{R_n}\sigma_{ij}); \quad R_n = R_1 \text{ or } R_2 \tag{1}$$

In Eq. (1), σ_{ij} and Π_{ij} terms are the stress components and the so-called piezospectroscopic coefficients, respectively. The equation simplifies if the reference orthogonal frame is chosen so that its axes coincide with the *a*, *m* and *c* axes of the reference hexagonal lattice[2,6]:

$$\Delta\bar{\nu}_{R_n} = \sum_{i=1}^{3} (\Pi_{i}^{R_n}\sigma_{i}) \tag{2}$$

In Eq. (2), the engineer notation ($i = 1$, 2 and 3 for 11, 22 and 33 indexes, respectively) has been adopted for simplicity and we shall use it from now on. He and Clarke[6] calibrated Eq. (2) (see Table 1) and confirmed the absence of shear stress wavenumber sensitivity in the specified frame. Their results have been widely used for *in situ* stress measurements in alumina-containing materials, including in DSEs.[2,7]

* Corresponding author. Tel.: +33 1 49 78 11 07; fax: +33 1 49 78 11 23.
E-mail address: gwenael.gouadec@upmc.fr (G. Gouadec).

0955-2219/$ – see front matter © 2012 Elsevier Ltd. All rights reserved.
doi:10.1016/j.jeurceramsoc.2012.01.038

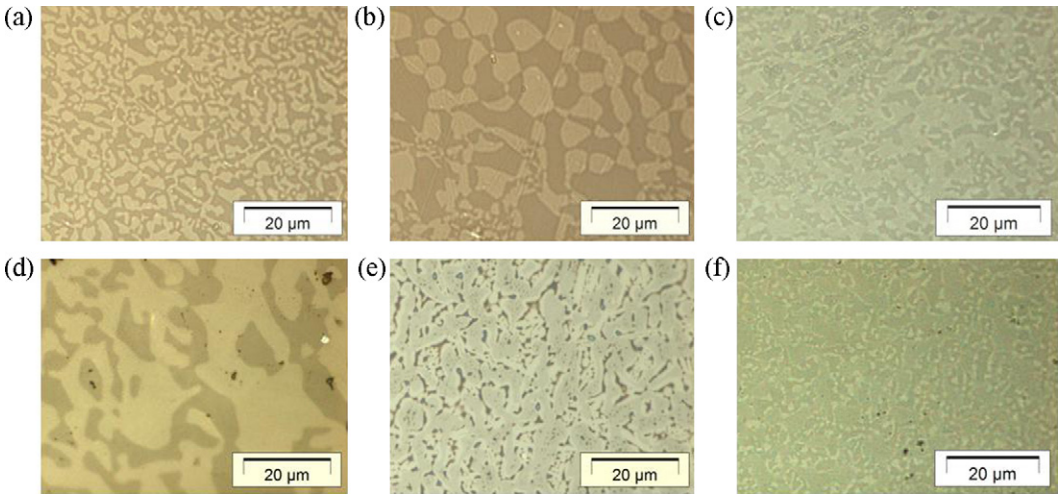

Fig. 1. Optical micrographs of polished cross sections from (a) AG sample (center of the rod), (b) AG (periphery of the rod), (c) AGZ, (d) AE, (e) AY and (f) AYZ. Alumina appears as the darkest phase.[30] Cubic zirconia is not clearly visible but was evidenced by XRD and EDX chemical cartography.[47] Refer to Table 2 for sample details.

This paper presents ruby fluorescence-based residual stress measurements in DSEs associating α-alumina with either $GdAlO_3$ perovskite (GAP), $Er_3Al_5O_{12}$ garnet (EAG) or $Y_3Al_5O_{12}$ garnet (YAG). Ternary eutectic compositions adding a cubic zirconia phase for increased flexural strength and fracture toughness[8,9] were also investigated. The present work being the first to study as many as six different DSEs at once, it gives a good insight on the intrinsic accuracy of the technique. Note that ruby Raman spectra exhibit stress sensitivity[10,11] (combined Raman and fluorescence piezospectroscopic studies have even been reported[12,13]) but the fluorescence is much easier to detect, specially in multiphased samples. Y^{3+}, Er^{3+} and Gd^{3+} ions fluorescence could in theory be used to measure stress in YAG, EAG and GAP phases, but rare-earth ions have a much lower stress sensitivity than transition elements.[6] The stress sensitivity of Cr^{3+} impurities fluorescence has been measured in GAP[14] but we could not detect a nice enough fluorescence signal to use it.

2. Materials and methods

2.1. The samples of the study

The acronyms for the samples are given in Table 2. The synthesis started with a 150 MPa isostatic pressing of cylinders (approximately 40 mm in length and 8 mm in diameter) formed with mixed 99.9% purity polycrystalline powders of Al_2O_3 (Baikowski Chimie, France), Gd_2O_3 (Rhodia, France), Er_2O_3 (Rhodia), Y_2O_3 (Rhodia) and ZrO_2 (Th. Goldschmidt Industriechemikalien, Germany). Two cylinders were then sintered for 10 h at 1673 K and later set in an arc image furnace operating with a 6 kW xenon lamp. As soon as a liquid droplet was obtained at the focal point of two elliptic mirrors, the cylinders were driven down at the constant speed of 10 mm h^{-1}. 3 mm-sided cubes were cut in the as-prepared rod centers and one face corresponding to the rod cross section was polished to 0.25 µm using diamond paste and colloidal silica. SEM and optical pictures show an interconnected structure[15] (Fig. 1) and α-alumina preferential orientation was revealed through TEM and electron backscattering diffraction[15,16] (Fig. 2). Like in most DSE rods, the cross sections exhibit a radial phase distribution (resulting from thermal gradients during synthesis) and a

Table 1
Alumina piezospectroscopy coefficients obtained by linear regression of data collected up to 0.9 GPa.[6] The original values were rounded to the first decimal place. $\Pi_{11}^{R_1}$ corresponds to the best linear fit of $\Delta\bar{\nu}_{cm^{-1}} = -2.56\sigma_{GPa} - 0.8\sigma_{GPa}^2$ relationship.[6]

Ruby line	Π_{11} (cm^{-1} GPa^{-1})	Π_{22} (cm^{-1} GPa^{-1})	Π_{33} (cm^{-1} GPa^{-1})
R_1	3.1	3.5	1.5
R_2	2.7	2.8	2.2

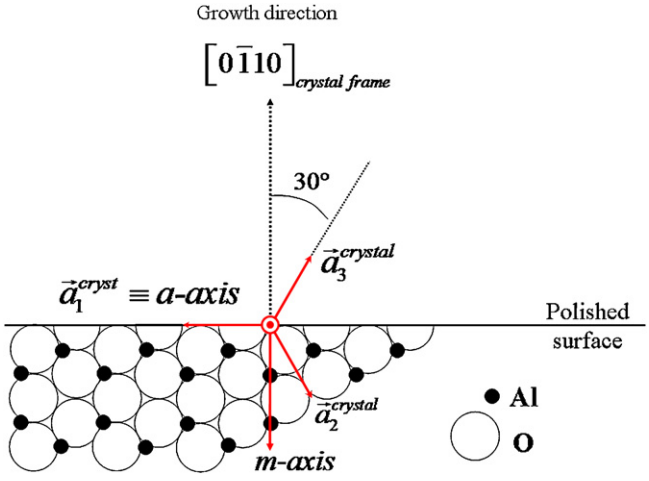

Fig. 2. α-Al_2O_3 preferential growth direction in all samples, as obtained through electron backscattering diffraction (EBSD) and transmission electron microscopy (TEM).[15,16] The polished surface is a cross-section of the eutectic rod. The *a*- and *m*-axes are the first two axes of the orthogonal frame used for ruby piezospectroscopy.

Table 2
The directionally solidified eutectic (DSE) samples of the study.[15,29,46,47]

Sample code	Starting batch	Melting temperature	X-ray phase analysis
AE	82 mol% Al_2O_3 18 mol% Er_2O_3	1810 °C	α-Al_2O_3 + $Er_3Al_5O_{12}$ (EAG)
AG	77 mol% Al_2O_3 23 mol% Gd_2O_3	1720 °C	α-Al_2O_3 + $GdAlO_3$ (GAP)
AY	81 mol% Al_2O_3 19 mol% Y_2O_3	1825 °C	α-Al_2O_3 + $Y_3Al_5O_{12}$ (YAG)
AEZ	65.9 mol% Al_2O_3 15.5 mol% Er_2O_3 18.6 mol% ZrO_2	–	α-Al_2O_3 + EAG + cubic ZrO_2
AGZ	58 mol% Al_2O_3 19 mol% Gd_2O_3 23 mol% ZrO_2	1700 °C	α-Al_2O_3 + GAP + cubic ZrO_2
AYZ	65 mol% Al_2O_3 16 mol% Y_2O_3 19 mol% ZrO_2	1715 °C	α-Al_2O_3 + YAG + cubic ZrO_2

α-Al_2O_3: trigonal alumina, EAG and YAG: cubic erbium and yttrium aluminum garnets and GAP: orthorhombic gadolinium aluminum perovskite.

number of structural imperfections occurring every few tens of micrometers.[12,17–20]

2.2. Ruby piezospectroscopy

Ruby fluorescence was observed with Raman microspectrometers, in air-conditioned rooms (for temperature stability) and using the 514.529 nm excitation of an Ar^+ ion laser. Cr^{3+} substitution by alumina soluble impurities is known to affect R-lines wavenumber[21] but we shall assume Cr^{3+} concentration to be the same in the alumina phase of all samples. Most spectra were collected on an "XY" model (Horiba-JY, formerly Dilor, France) equipped with a double monochromator as a filter and a back-illuminated 2000 × 800 pixels CCD detector cooled down to 140 K in liquid nitrogen. Because of a temporary unavailability of the XY model, AEZ sample was studied with a Labram-HR (Horiba-JY) spectrometer. We systematically used 100× objectives (~1 μm diameter lateral probing) to select perfectly homogeneous domains and avoid the structural disturbances described in Section 2.1. The emission from a neon lamp was used to serve as an external reference and we will refer to the 703.24 and 692.95 nm lines[22] as Ne_1 and Ne_2, respectively. "Raman shifts" measuring the wavenumber difference between the photons collected from a laser-illuminated sample and those from the source, R_1 ($\lambda = 694.2$ nm) and R_2 ($\lambda = 692.8$ nm) lines show around 5000 cm^{-1} with a 514.5 nm laser (Fig. 3).

3. Results and discussion

All the tested DSEs have R_1 and R_2 fluorescence bands peaking at lower absolute wavenumber (higher Raman shift) than in a stress-free ruby (Fig. 3), revealing an overall compression of alumina phase.[6] A preliminary fitting of a large series of neon spectra such as the one shown in Fig. 3 established that Ne_1 and Ne_2 lines have a Gaussian shape, that Ne_2 has a width of 1.95 cm^{-1} and that its intensity is 30% that of Ne_1. We used these parameters to fit a large number of fluorescence spectra twice, with or without taking Ne_2 component into consideration. There was no consequence on R_1 pinpointing and R_2 wavenumber changed by less than 0.1 cm^{-1} whenever R_1 intensity was at least 6 times that of Ne_1 (Fig. 4). From now on, we shall therefore restrict our study to spectra recorded with $I(R_1)/I(Ne_1) \geq 6$ (*i.e.* $I(R_2)/I(Ne_2) \geq 12.5$) and fitted without Ne_2 component.

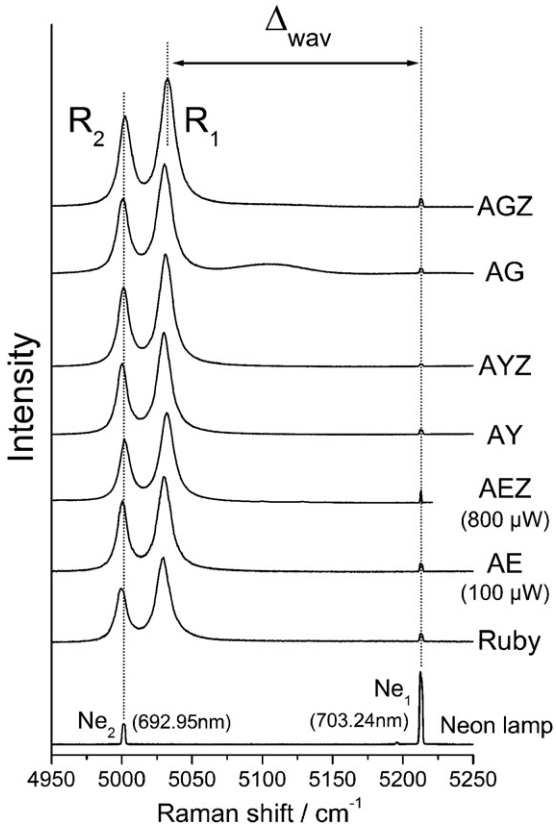

Fig. 3. Ruby fluorescence (R_1 and R_2 bands) excited with a 514,529 nm laser. Unless stated, the power of illumination was 6 mW. Neon lines Ne_1 and Ne_2 are used as absolute references.

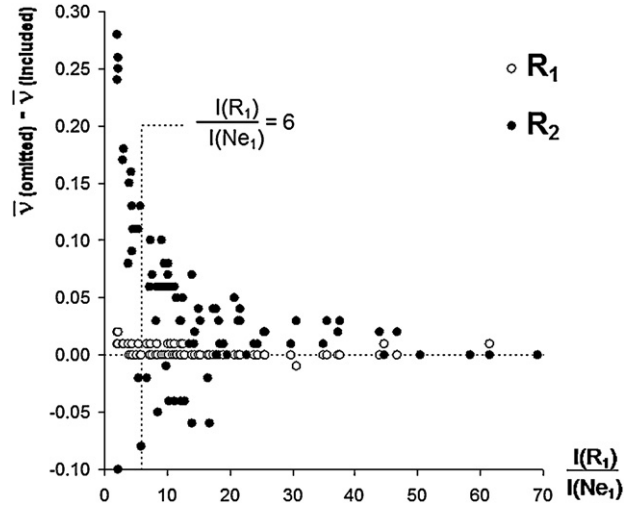

Fig. 4. Variation of R_1 and R_2 fitted wavenumber (in cm^{-1} unit) depending on whether Ne_2 line is included or omitted in the fitting procedure. $I(R_1)/I(Ne_1)$ is the intensity ratio of R_1 and Ne_1 lines.

A $\sim 0.15\,cm^{-1}\,K^{-1}$ thermal shift was measured on ruby samples probed at different temperatures.[6,23–25] A preliminary testing of our DSE samples showed no shift of R-lines for any laser power below 1 mW (measured on the sample) and less than $0.5\,cm^{-1}$ overall shift for a power of 20 mW. Laser illumination thus provokes almost no heating. We limited the incident power (as measured on the sample) to 6 mW or less and Fig. 5 confirms the limited influence of the actual value on R_1 and R_2 pinpointing. With the possible exception of AGZ (only two powers were tested), there is indeed no systematic drift with a power change. The scattering of Δ_{wav} (as defined in Fig. 3) is above the precision of R_1 pinpointing (reaching about $1.3\,cm^{-1}$ when AG sample is probed at 0.5 or 6 mW). There is therefore some variability from one point of a sample to another (not to mention the distribution of stress throughout each alumina grain, as was

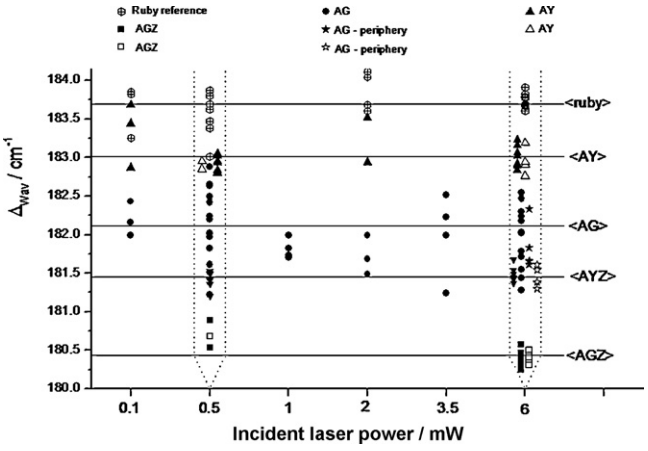

Fig. 5. Fitted values of Δ_{wav} (Fig. 3) as a function of the incident power measured on the sample (some series recorded with 0.5 and 6.0 mW were shifted for better viewing). The fluorescence spectra were recorded with the laser focused on optically dark domains (alumina) except for the series marked with hollow symbols (laser focused on the garnet or perovskite phase). The periphery of AG sample is characterized by a coarser microstructure (see Fig. 1a and b). Horizontal lines indicate each series average value.

observed with near field setups in alumina polycrystals[26] and Al_2O_3/ZrO_2 eutectics[19]).

Even though the $\sigma_1 = \sigma_2 \neq \sigma_3$ stress field hypothesis was tested on occasion,[19,27,28] the assumption that a purely hydrostatic stress σ_H is measured is the most widely used to convert ruby shifts into residual stress:

$$\sigma_H = \frac{\Delta\bar{\nu}_{R_n}}{\Pi_1^{R_n} + \Pi_2^{R_n} + \Pi_3^{R_n}} \quad (3)$$

Such assumption probably makes sense in the bulk of our samples because they are homogeneous (phases alternate every few microns (Fig. 1) when the side of the cubic samples is ~3 mm) and isotropic (longitudinal and transversal cross sections look very much the same[15,29]). However, the possibility for a surface-related disturbance must be discussed. Indeed, even though the samples are translucent (they illuminate under laser irradiation and mixed alumina/rare-earth oxide Raman contributions are systematically observed[30]), the laser is focused through a microscope objective. In air, the depth of focus (classically defined as the distance along the optical axis z where irradiance remains above 50% of its maximum value) is approximately $4\lambda/NA^2$, NA being the numerical aperture.[31,32] This corresponds to only 2.5 μm in our conditions ($\lambda = 514.5$ nm; NA = 0.9). Even though the depth of focus is significantly degraded by refractions (at the air/sample and inner sample interfaces) when light penetrates solids,[31,33–36] it thus appears that most of the collected signal comes from the first 10 μm below the surface of our samples. In such rigid materials as DSEs (ceramics in general), one may argue that stress builds up over limited distances and bulk conditions must extend close to the free surface. Yet, we obtained different wavenumbers in AG periphery (where the domains are the largest (Fig. 1)) depending on whether alumina was probed directly or through GAP (Fig. 5). It therefore seems that there is some surface specific contribution to the ruby fluorescence signal we detected. It has to be limited though since Harlan et al. reported no significant change of ruby lines when a macroscopic setup (parallel beam) was used instead of a microscope (focused beam) to analyze alumina/zirconia eutectics.[28] Besides, their results were in accordance with calculations based on a triaxial stress state hypothesis. Unfortunately we could not test the macroscopic setup alternative on our own samples because they are heterogeneous at the scale of a few tens of micrometers and it would have meant probing different morphologies at once.

In the piezospectroscopy frame of Fig. 2, a purely planar stress field with $\sigma_2 = 0$ should best describe the vicinity of the sample surface. If we assume isotropy ($\sigma_1 = \sigma_3 = \sigma_P$), Eq. (2) leads to:

$$\sigma_P = \frac{\Delta\bar{\nu}_{R_n}}{\Pi_1^{R_n} + \Pi_3^{R_n}} \quad (4)$$

Fig. 6 and Table 3 give the residual stress calculated using Table 1 values in the hydrostatic (Eq. (3)) and planar equibiaxial (Eq. (4)) stress models. The (average) error bars were calculated using the following uncertainties:

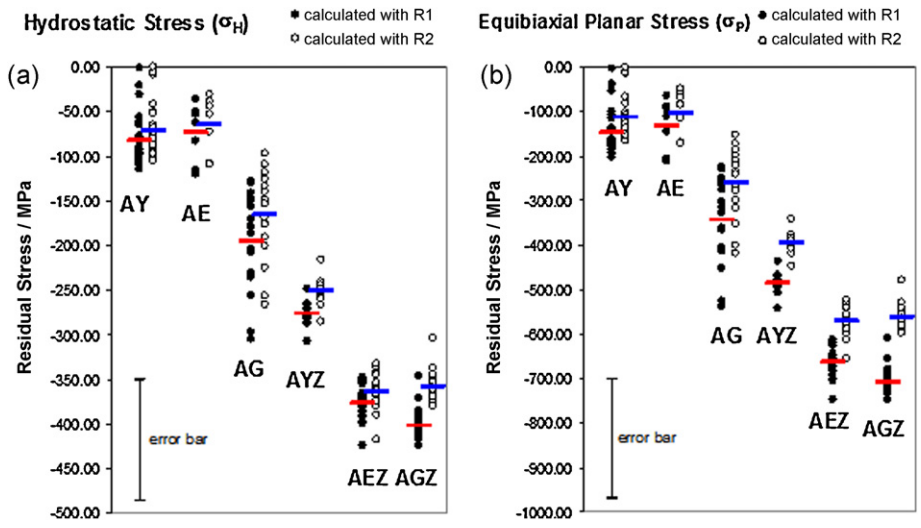

Fig. 6. The residual stress calculated according to Eqs. (3) and (4). The fluorescence spectra were recorded with the laser focused on optically dark domains (alumina). The horizontal bars are average values.

Table 3
Average residual compression calculated in alumina phase based on fluorescence spectra verifying the condition $(I_{R_1}/I_{Ne_1}) \geq 6$. Hydrostatic ($\sigma_H$) and planar equibiaxial (σ_P) assumptions were tested (see text).

Sample	σ_H (MPa)		σ_P (MPa)		Prev. σ_H (MPa)
	R_1	R_2	R_1	R_2	
AE	−75	−65	−130	−105	−135[48]
AEZ	−375	−365	−665	−570	
AY	−85	−70	−145	−115	−100[18]
AYZ	−275	−250	−485	−395	−300[a,49] [−300;−400][18]
AG	−195	−165	−345	−260	
AGZ	−400	−360	−710	−560	

[a] At a comparable growth rate.

- 0.1 cm^{-1} GPa^{-1} for all piezospectroscopic coefficients except $\Pi_{11}^{R_1}$. For the latter we took 0.4 cm^{-1} GPa^{-1} uncertainty since the slopes letting He and Clarke experimental data points[6] above and below a straight line would be −2.6 and −3.3 cm^{-1} GPa^{-1}, respectively.
- 0.2 cm^{-1} for R_1 and R_2 wavenumber shifts. Each line was indeed positioned with the ∼0.1 cm^{-1} fitting-related uncertainty evidenced in Fig. 4, the use of Ne_1 reference compensating for the uncertainty on the spectrometer positioning.

In Fig. 6b, the σ_P values derived from R_1 and R_2 lines agree to within error bars. The use of Eq. (4) to assess the non hydrostatic component of the stress field is thus probably legitimate. Unfortunately, the "random" distribution of alumina precludes the testing of hypothesized depth-dependent combinations of σ_H and σ_P to simulate the experimental ruby shifts.[37,38] The best way to assess at which depth the stress field becomes purely hydrostatic would be to close the confocal hole of the Raman microscope (thus reducing the depth of field) and progressively lower laser focus into the sample down to the level where the ruby lines would show no variation. This is far beyond the original scope of this study because a thorough statistical approach would be mandatory to smooth the effect of the random alumina distribution across the sample thickness, not to mention the problem of refraction altering the actual probing depth.[31,33–36]

There is little agreement between our σ_H values and those previously reported in AY, AYZ and AEZ samples (Table 3). Yet, there is no way of being sure that the samples and conditions of analysis were strictly equivalent. We obtain small residual stresses in AE and AY binary eutectics, as expected from the close thermal expansion coefficients of the garnet and alumina phases (Table 4). Values below 250 MPa were already found in $Al_2O_3/Y_3Al_5O_{12}$ eutectics based on X-ray diffraction experiments (triaxial stress field)[39,40] and indentation fracture tests (hydrostatic hypothesis)[41]. In AG sample, the stress level is higher and a compression of alumina is ascertained, even

Table 4
Thermal expansion coefficients (in units of 10^{-6} K^{-1}) as obtained from dilatometry[30] and X-ray diffraction[29] experiments for temperatures up to 1000 K. (s): single crystal; (p): polycrystalline.

Trigonal Al_2O_3 (s)	Dilato.: $\alpha_a = 8.7/\alpha_c = 9.3$ XRD: $\alpha_a = 7.8/\alpha_c = 8.7$
$Er_3Al_5O_{12}$ garnet (p)	$\alpha_{dilato.} = 9.0$ $\alpha_{XRD} = 7.9$
$Y_3Al_5O_{12}$ garnet (p)	$\alpha_{dilato.} = 8.8$ $\alpha_{XRD} = 8.5$
$GdAlO_3$ perovskite (p)	$\alpha_{dilato} = 7.7$ XRD: $\alpha_a = 10.1/\alpha_b = 3.9/\alpha_c = 8.0$

taking the error bars into account. Again regardless of the model, the residual compression is at least doubled in each ternary sample by comparison with the zirconia-free counterpart. The high CTE of yttria-stabilized cubic zirconia (between 11.2 and $12.9 \times 10^{-6}\,K^{-1}$ according to Refs. 42–44, cited in Brewer et al.[45]) is a logical explanation for this behavior.

4. Conclusions

Ruby fluorescence was used to measure the residual compression of the alumina phase in melt-grown directionally solidified eutectic composites associating gadolinum aluminum perovskite (GAP), erbium aluminum garnet (EAG) or yttrium aluminum garnet (YAG) with α-alumina and cubic zirconia. Alumina residual compression depends on the second phase with $\sigma(Al_2O_3–GAP) > \sigma(Al_2O_3–YAG) \sim \sigma(Al_2O_3–EAG)$ and raises when cubic-zirconia is added as a third phase. Our results suggest that the stress field that is probed with microscopes is not purely hydrostatic because of a surface specific planar contribution in the probed volume.

Acknowledgment

The authors are grateful to Dr. Michel Parlier from the Department of Materials and Composite Structures (DMSC) at ONERA.

References

1. Waku Y. High temperature characteristics of melt growth composites and their application to ultra high efficiency gas turbine components. *Key Eng Mater* 2006;**317–318**:473–80.
2. LLorca J, Orera VM. Directionally solidified eutectic ceramic oxides. *Prog Mater Sci* 2006;**51**:711–809.
3. Lakiza SM. Directionally solidified eutectics in the $Al_2O_3–ZrO_2–Ln(Y)_2O_3$ systems. *Powder Metall Met Ceram* 2009;**48**:42–59.
4. Mao HK, Xu J, Bell PM. Calibration of the ruby pressure gauge to 800 kbar under quasi-hydrostatic conditions. *J Geophys Res* 1986;**91**: 4673.
5. Grabner L. Spectroscopic technique for measurement of residual stress in sintered Al_2O_3. *J Appl Phys* 1978;**49**:580–3.
6. He J, Clarke DR. Determination of the piezospectroscopic coefficients for chromium-doped sapphire. *J Am Ceram Soc* 1995;**78**:1347–53.
7. Oliete PB, Peña JI, Llarea A, Orera VM, Llorca J, Pastor JY, et al. Ultra-high-strength nanofibrillar Al_2O_3–YAG–YSZ eutectics. *Adv Mater Opt Electron* 2007;**19**:2313–8.
8. Hirano K. Application of eutectic composites to gas turbine system and fundamental fracture properties up to 1700 °C. *J Eur Ceram Soc* 2005;**25**:1191–9.
9. Waku Y, Sakata S, Mitani A, Shimizu K, Ohtsuka A, Hasebe M. Microstructure and high-temperature strength of $Al_2O_3/Er_3Al_5O_{12}/ZrO_2$ ternary melt growth composite. *J Mater Sci* 2005;**40**:711–7.
10. Jia W, Yen WM. Raman scattering from sapphire fibres. *J Raman Spectrosc* 1989;**20**:785–8.
11. Shin SH, Pollak FH, Raccah PM. Effects of uniaxial stress on the Raman frequencies of Ti_2O_3 and Al_2O_3. In: *3rd Inter. Conf. on Light Scattering in Solids*. 1975.
12. Pardo JA, Merino RI, Orera VM, Peña JI, González C, Pastor JY, et al. Piezospectroscopic study of residual stresses in $Al_2O_3–ZrO_2$ directionally solidified eutectics. *J Am Ceram Soc* 2000;**83**:2745–52.
13. Ohtsuka S, Zhu W, Tochino S, Sekiguchi Y, Pezzotti G. In-depth analysis of residual stress in an alumina coating on silicon nitride substrate using confocal Raman piezo-spectroscopy. *Acta Mater* 2007;**55**:1129–35.
14. Jovanic BR, Andreeta JP. Effects of high pressure on the fluorescence spectra of Cr^{3+} in $GdAlO_3$. *J Phys Condens Matter* 1998;**10**:271–4.
15. Mazerolles L, Perrière L, Lartigue-Korinek S, Piquet N, Parlier M. Microstructures, crystallography of interfaces, and creep behavior of melt-growth composites. *J Eur Ceram Soc* 2008;**28**:2301–8.
16. Piquet N. *Microstructures Interconnectées dans des Eutectiques à base d'Oxydes Réfractaires Elaborés par Solidification Dirigée*. Créteil: Univ. Paris 12 Val de Marne; 2006. p. 198.
17. Orera VM, Cemborain R, Merino RI, Peña JI, Larrea A. Piezo-spectroscopy at low temperatures: residual stresses in $Al_2O_3–ZrO_2(Y_2O_3)$ eutectics measured from 77 to 350 K. *Acta Mater* 2002;**50**:4677–86.
18. Larrea A, Orera VM, Merino RI, Peña JI. Microstructure and mechanical properties of Al_2O_3–YSZ and Al_2O_3–YAG directionally solidified eutectic plates. *J Eur Ceram Soc* 2005;**25**:1419–29.
19. Fukura S, Kagi H, Nakai M, Sugiyama K, Fukuda T. High-resolution stress mapping of Al_2O_3/monoclinic ZrO_2 and Al_2O_3/cubic $ZrO_2(Y_2O_3)$ eutectics using scanning near-field optical microscopy. *J Cryst Growth* 2009;**311**:998–1004.
20. Gouadec G, Colomban Ph, Piquet N, Trichet M-F, Mazerolles L. Raman/Cr^{3+} fluorescence mapping of a melt-grown $Al_2O_3/GdAlO_3$ eutectic. *J Eur Ceram Soc* 2005;**25**:1447–53.
21. Yu H, Clarke DR. Effect of codoping on the R-line luminescence of Cr^{3+}-doped alumina. *J Am Ceram Soc* 2002;**85**:1966–70.
22. Saloman EB, Sansonetti CJ. *J Phys Chem Ref Data* 2004;**33**:1113–58.
23. Jahren AH, Kruger MB, Jeanloz R. Alexandrite as a high-temperature pressure calibrant, and implications for the ruby-fluorescence scale. *J Appl Phys* 1992;**71**:1579–82.
24. Gibson UJ, Chernuschenko M. Ruby films as surface temperature and pressure sensors. *Opt Express* 1999;**4**:443–8.
25. Nychka JA, Clarke DR. Damage quantification in TBCs by photostimulated luminescence spectroscopy. *Surf Coat Technol* 2001;**14**:6–147, 110-6.
26. Narita Y, Murotani H. Submicrometer optical characterization of the grain boundary of optically active Cr^{3+} doped polycrystalline Al_2O_3 by near-field spectroscopy. *Am Mineral* 2002;**87**:1144–7.
27. He J, Clarke DR. Polarization dependance of the Cr^{3+} R-line fluorescence from sapphire and its application to crystal orientation and piezospectroscopic measurement. *J Am Ceram Soc* 1997;**80**:69–78.
28. Harlan NR, Merino RI, Peña JI, Larrea A, Orera V, Gonzalez C, et al. Phase distribution and residual stresses in melt-grown $Al_2O_3–ZrO_2(Y_2O_3)$ eutectics. *J Am Ceram Soc* 2002;**85**:2025–32.
29. Perrière L. *Elaboration par Solidification Dirigée et Comportement Mécanique de Céramiques Eutectiques à base d'Oxydes Réfractaires. Rôle de la Microstructure sur la Fissuration et la Déformation Plastique à Haute Température*. Créteil: Univ. Paris 12 – Val de Marne; 2008.
30. Gouadec G, Makaoui K, Perrière L, Colomban Ph, Mazerolles L. Polarized micro-Raman study of Al_2O_3-based directionally solidified oxide eutectics containing $GdAlO_3$ perovskite, $Er_3Al_5O_{12}$ garnet and cubic ZrO_2. *J Raman Spectrosc* 2010;**41**:969–77.
31. Bruneel J-L, Lassègues J-C, Sourisseau C. In-depth analysis by confocal Raman microspectroscopy. *J Raman Spectrosc* 2002;**33**:815–28.
32. Inoué S. Foundations of confocal scanned imaging in light microscopy. In: Pawley JB, editor. *Handbook of biological confocal microscopy*. 3rd ed. New York: Springer Science+Business Media; 2006.
33. Tomba JP, de-la-Paz-Miguel M, Perez CJ. Correction of optical distortions in dry depth profiling with confocal Raman microspectroscopy. *J Raman Spectrosc* 2010;**42**:1330–4.
34. Everall NJ. Confocal Raman microscopy: why the depth resolution and spatial accuracy can be much worse than you think. *Appl Spectrosc* 2000;**54**:1515–20.
35. Everall NJ. Modeling and measuring the effect of refraction on the depth resolution of confocal Raman microscopy. *Appl Spectrosc* 2000;**54**: 773–82.
36. Guo S, Todd RI. Confocal fluorescence microscopy in alumina-based ceramics: where does the signal come from? *J Eur Ceram Soc* 2010;**30**:641–8.

37. Atkinson A, Jain SC. Spatially resolved stress analysis using Raman spectroscopy. *J Raman Spectrosc* 1999;**30**:885–91.
38. Zhu W, Pezzotti G. Raman analysis of three-dimensionally graded stress tensor components in sapphire. *J Appl Phys* 2011;**109**:073502.
39. Dickey EC, Frazer CS, Watkins TR, Hubbard CR. Residual stresses in high-temperature ceramic eutectics. *J Eur Ceram Soc* 1999;**19**:2503–9.
40. Sha JJ, Ochiai S, Okuda H, Waku Y, Nakagawa N, Mitani A, et al. Residual stresses in YAG phase in directionally solidified eutectic Al_2O_3/YAG ceramic composite estimated by X-ray diffraction. *J Eur Ceram Soc* 2008;**28**:2319–24.
41. Ochiai S, Ikeda S, Iwamoto S, Sha JJ, Okuda H, Waku Y, et al. Residual stresses in YAG phase of melt growth Al_2O_3/YAG eutectic composite estimated by indentation fracture test and finite element analysis. *J Eur Ceram Soc* 2008;**28**:2309–17.
42. Terblanche P. Thermal-expansion coefficients of yttria-stabilized cubic zirconias. *J Appl Crystallogr* 1989;**22**:283–4.
43. Karaulov AG, Zoz EI, Rudyaki N, Sudarkina TE. Structure and properties of solid solutions in the systems: ZrO_2–MgO, ZrO_2–CaO, and ZrO_2–Y_2O_3. *Refractories* 1983;**24**:452–8.
44. Touloukian YS. Oxides and their solutions and mixtures. In: *Thermophysical properties of high temperature solid materials.* New York: Macmillan; 1967. p. 970.
45. Brewer LN, Peascoe RA, Hubbard CR, Dravid VP. Residual stress distributions in the solid solution eutectic $Co_{1-x}Ni_xO/ZrO_2$(CaO). *J Am Ceram Soc* 2003;**86**:2188–94.
46. Perrière L, Valle R, Mazerolles L, Parlier M. Crack propagation in directionally solidified eutectic ceramics. *J Eur Ceram Soc* 2008;**28**:2337–43.
47. Mazerolles L, Piquet N, Trichet MF, Perrière L, Boivin D, Parlier M. New microstructures in ceramic materials from the melt for high temperature applications. *Aerosp Sci Technol* 2008;**12**:499–505.
48. Mesa MC, Oliete PB, Orera VM, Pastor JY, Martín A, L.Lorca J. Microstructure and mechanical properties of $Al_2O_3/Er_3Al_5O_{12}$ eutectic rods grown by the laser-heated floating zone method. *J Eur Ceram Soc* 2011;**31**:1241–50.
49. Peña JI, Larsson M, Merino RI, de Francisco I, Orera VM, LLorca J, et al. Processing, microstructure and mechanical properties of directionally-solidified Al_2O_3–$Y_3Al_5O_{12}$–ZrO_2 ternary eutectics. *J Eur Ceram Soc* 2006;**26**:3113–21.